Tribological mechanisms involved in Friction Wood Welding

Pierre-Henri Cornuault[*], Luc Carpentier

Femto-ST Institute – Department of Applied Mechanics, UBFC, CNRS UMR 6174, Besançon, France

* corresponding author: pierre-henri.cornuault@ens2m.fr
+ 33(0)381402854

Abstract

Friction wood welding (FWW) is an innovative process allowing wooden parts to be joined without any external material addition. Surprisingly, whereas extensive investigations on chemical reactions involved in FWW were carried out, no tribological studies have ever been performed to characterize the underlying frictional mechanisms. This paper addresses this limitation through linear reciprocated friction tests performed on beech wood samples under various contact pressures and moisture contents. Tests results coupled with a characterization of surface modifications highlight the variety of frictional mechanisms. Ultimately, this study also suggests that the friction coefficient is a relevant tool in order to control the process in the goal of optimizing the mechanical strength of the welded assembly.

Keywords: wood; welding; tribology; surface modification

1   Introduction

The Friction Wood Welding (FWW) process was first discovered and then patented by Sutthoff[1] in 1996. The first studies seeking to understand the physical phenomena involved in FWW were then published since 2003 by Gfeller and Pizzi et al.[2,3] FWW is tribologically driven since it is achieved by the relative displacement of two wooden parts under normal contact pressure. The frictional heat generated at the contact interface induces local transformation of wood into a molten material which then solidifies to form a strong joint. The relevance of the process relies on joining wooden parts without any external material addition such as glue, resulting in totally environment-friendly assemblies. While ultrasonic and friction stir welding techniques applied to wooden materials show strong potential[4], FWW was mainly achieved under two geometric configurations: cylinder-in-block conformal contact and plane-on-plane contact. Usually named rotation welding[5], the first configuration refers to the rotating friction of wood dowels into pre-drilled, or not[6], wooden blocks. On the other hand, plane-on-plane FWW was firstly achieved through planar orbital motion[7,8] by analogy with the welding of thermoplastics, but it was durably supplanted by reciprocated linear motion usually named linear (or vibrational) welding.[2,9] Linear welding corresponds to the most published wood welding option and is the scope of the present study. Notwithstanding, one can notice that similar phenomena and material modifications were observed in both linear, orbital and rotation welding.[5,6]

Linear FWW was successfully performed with various wood species including beech[2,10–13] spruce[11,14–16], oak[9,11,13] pine[17–19], birch[20,21], poplar[21], maple[13], eucalyptus[22–24], bamboo[25,26], and even heat-treated woods[21,27]. Nevertheless, softwood welding appeared to be more difficult to achieve due to the characteristic cell-wood collapsing effect of these species.[11] While FWW were sometimes achieved through multi-pass contact conditions[9,22,23,25,26,28–30], the process is carried out in a few seconds through two successive steps. First, friction is carried out under specific contact conditions including welding pressure (WP), sliding velocity (SV), displacement amplitude (DA), and welding time (WT). Second, the contact is maintained under static mechanical loading defined by the holding pressure (HP) and the holding time (HT). Based on numerous studies[2,9,25–34,10,35–37,11,15,20–24], WP ranges from 0.2 to 4.5 MPa, DA remains close to 2 mm, WT is very short and ranges from 1 to 8 s, HP from 1 to 8 MPa, and HT

from 5 to 60 s. The sliding speed is classically expressed as a motion frequency which ranges from 100 to 150 Hz, leading to *SV* close to 0.6 m.s⁻¹ when considering the associated *DA* value.

Since the frictional heating of surfaces drives the material modification, it was studied by inserting thermocouples in the contact during the process[2,25] or by infrared thermography measurements[31]. Maximal temperatures ranging from 200 to 350°C were measured, depending on wood species and contact conditions. Moreover, finite element method (FEM) models based on thermal conduction and convection assumptions confirmed these values.[18,38] It is worth mentioning that the thermal loading remains located in the close vicinity of the contact since measurements carried out in the bulk wood and only 1 mm away from the interface led to temperatures close to the ambient one.[2] This essential feature explains the absence of wood parts distortion far from the contact zone, leading to a high quality assembly. Heat also has a major impact on the chemistry inside the contact.

Chemical reactions resulting from temperature increases during FWW were in-depth characterized in detail in elaborate studies[31,39] focused on modifications of the three main thermoplastic constituents of wood: cellulose, hemicellulose, and lignin. Complex interactions between multiple hydrolysis and condensation reactions take place with the elevation of temperature. They are driven by successive consumptions and productions of water molecules. On the one hand, some of these reactions are exothermic leading to a further increase of the temperature[31] catalysing themselves. On the other hand, water evaporation and material ejection from the contact tend to cool the system.[38] Most of chemical reactions involved in FWW occur at the beginning of the process resulting in furfural production, extensive degradation of hemicellulose, increases of crystallinity and intramolecular bonding of cellulose which remains only slightly degraded at this stage and, above all, lignin fusion.[39] Evidence of lignin melting and hemicellulose degradation[2] were also supported by the analysis of gases emitted during the process.[34,40] As soon as lignin is molten, it inhibits the continuation of these transformations and has a protective effect on cellulose degradation.[39] Meanwhile, wood pyrolysis generates charcoal.[31] Then, lignin cross-linking, and partial networking between lignin and cellulose occur and continue even after the motion is stopped.[39] At the end of the process, cellulose depolymerisation leads to the partial destruction of the cell-wood walls. FWW ultimately results in a densified melting zone (MZ) located at the wooden parts interface.[11] Scanning electron microscopy (SEM) observations of the MZ revealed a complex network of entangled wood fibres (tracheids) embedded in a matrix of molten and then cured material mainly composed of lignin.[2,31] Local modification of mechanical properties such as increase of hardness and elastic recovery[14] were reported. The cross-sectional width of the densified MZ ranges from 100 µm to approximately 2 mm depending on wood species[11,31] and welding parameters such as *WP* and *WT*.[19]

The resulting mechanical strength of the welded wood assembly depends consistently on the wood species[22,23], *WT*[9,16,20], *WP*[16,22], *SV* and *DA*[22], wood grain orientation[9], and on the original surface topography.[10,15] Moreover, larger *HT* results in higher strength due to continuous increase of material cross-linking after the motion is stopped.[2,31,39] Shear strength ranging from 1.8 to 13.4 MPa[9,22,23,29,31] and tensile strength ranging from 0.5 to 10.5 MPa[2,9,12,20,21,24] were reached depending on the abovementioned welding conditions.

Despite the high level of knowledge accumulated concerning the chemical reactions involved in FWW, the multiple effects of wood species and welding parameters on the resulting MZ features and mechanical properties, tribology-focused studies of FWW have never been conducted so far. Very surprisingly, and to the best of our knowledge, only one publication has dealt with measurements of the coefficient of friction (COF) between wooden parts during the process.[8] It was focused on orbital welding while this option has been progressively replaced by linear FWW. Moreover, limited confidence can be placed on the COF values provided since both the measurements and the post-processing methods remained imprecisely described in this paper. Notwithstanding, the authors

2

observed an inverted U-shaped evolution of the friction force throughout the process. Minimal COF lower than 0.1 were reported at the beginning of the process, before reaching a maximal value close to 0.3. These typical COF values did not change when varying the contact pressure but appeared to increase when decreasing the orbital motion frequency, *i.e.* the sliding speed.[8] Even more intriguing ten-times lower COF values were deduced from heat-transfer numerical modelling.[18]

The present paper consequently addresses those limitations. The linear FWW process is studied for the first time through a tribological approach. The main objective of our study is to show that such an approach allows for further understanding FWW mechanisms, and even for controlling it. A fully instrumented tribometer is used to perform tests in relevant contact conditions with respect to FWW. An original approach coupling friction force measurements and surface modifications observation throughout the process is proposed.

2 Materials and methods

2.1 Selection and preparation of wood samples

Experiments were conducted with beech-wood (*Fagus sylvatica*) samples of two shapes: pin samples were cylinders of 8 mm in diameter and 20 mm in length, and block samples were cubes of $12 \times 14 \times 14$ mm³. Both sample types were extracted from the same sapwood tree and machined such that pin's circular base and block's larger face corresponded to the beech transversal cross-section. Figure 1 shows the samples' geometrical features, structure, and orientation. As a diffuse-porous wood specie, beech is a very heterogeneous material. Special attention was consequently paid to overcome excessive behavioural variations by selecting 47 pins and 47 blocks presenting similar structures among more than 100 samples of each geometry. The transversal cross-section of the selected pins and blocks exhibited a mean total number of growth rings equal to 3.4 and 6.9, respectively. Samples were stored in a dedicated glass jar where temperature (T) and relative humidity (RH) were maintained at $21 \pm 2°C$ and $39 \pm 5\%$, respectively. The calculated mean equilibrium moisture content (MC) of the samples was 11%. Among the 47 pin/block pairs studied, 5 of them were however heat-treated at 115°C during 2 hours to reach the anhydrous state ($MC = 0$). Five others pin/block pairs were immersed in distilled water during 2 hours and then dried at ambient air during 80 min (for blocks) or 125 min (for pins) in order they reached $MC = 25\%$.

2.2 Friction tests and further analyses

Friction tests were performed at room temperature and ambient air using a Cameron-Plint TE77 tribometer achieving pin-on-block linear reciprocated motion with a ± 2.2 mm displacement stroke at 50 Hz. Since the reciprocal linear motion was carried out through a rotative DC motor activating an eccentric-cam system, the pin displacement (h) followed a sinusoidal curve against time and the mean sliding velocity during each back-and-forth friction cycle is 0.44 m.s⁻¹. Due to the actuator inertia, it is worth mentioning that 14 friction cycles (*i.e.* 0.28 s) were necessary at the beginning of the tests to reach the abovementioned mean speed. Similarly, the decrease of the sliding speed from 0.44 m.s⁻¹ to 0 at the end of each test lasted 14 friction cycles also. The normal load (F_N) was applied on the pin/block contact through a tension spring. Throughout each test, the pin displacement, the friction force (F_T), and F_N were respectively measured thanks to a non-contact laser sensor, a piezoelectric sensor, and a gauge strain sensor. These 3 signals were acquired with a 10 kHz sampling frequency. For each friction cycle, the friction coefficient (μ) was calculated from an energetic point of view using Eq. 1 where the local friction coefficient (F_T / F_N ratio) is integrated throughout a single back-and-worth motion and where Δh_0 (very close to 4.4 mm) is the distance between the two pin positions corresponding to $F_T = 0$.

$$\mu = \frac{1}{2\,\Delta h_0} \int \left| \frac{F_T}{F_N} \right| dh \qquad (Eq.1)$$

3

When considered, the mean values of the normal load and the friction force throughout an overall friction cycle were respectively named $\overline{F_N}$ and $\overline{F_T}$.

For all friction tests, plane-on-plane contact geometry was used and the rubbing direction was set perpendicular to beech grains direction, perpendicular to growth rings, and parallel to wood-rays direction of both pin and block (Figure 1). This samples orientation thus corresponded to end grain-to-end grain butt welding reported in previous studies.[9,22,24,25] As described in the following subsections, three distinctive test campaigns were conducted according to different contact conditions, procedures, and post-testing analysis methods.
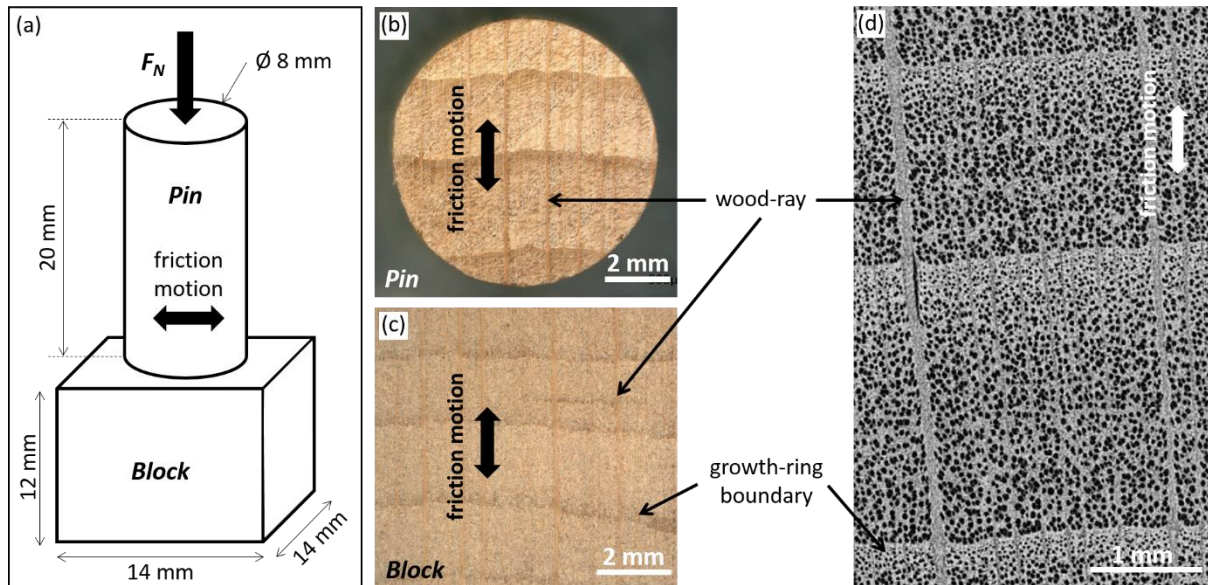
Figure 1:

Figure 1: Tribologic contact studied and samples geometry (a), microscope observation of the pin (b) and block (c) contacting surfaces, and typical cross-section reconstructed by X-ray tomography of the samples showing the diffuse-porous microstructure of beech wood (d).

2.2.1   Test campaign 1 (TC1): Friction coefficient related to contact conditions

Test campaign 1 was performed in the goal of characterizing the effect of *WP* and beech-wood *MC* on the evolution of μ versus the number of friction cycles (*N*). To this end, friction tests were performed under 1.5, 2.2, 3.0, and 3.8 MPa initial contact pressure (P_C) with samples having *MC* = 11%. Other tests were carried out on samples exhibiting *MC* = 0 and 25% with P_C = 3.0 MPa in each case. For all tested contact conditions, 5 tests were performed for reproducibility purposes. Different test durations ranging from *N* = 220 to 450 were carried out depending on contact conditions.

2.2.2   Test campaign 2 (TC2): Characterization of surface modifications

The objective of this test campaign was to characterize the pin/block interface modifications during FWW process. Friction tests were therefore interrupted at 3 different steps of the process, namely after *N* close to 60, 110, and 170 friction cycles. To prevent any joining of the pin/block interface, an external lever was used, allowing for opening the contact before the pin motion was even stopped. All tests were performed under the same contact condition corresponding to *MC* = 11% and P_C = 3.0 MPa, and 3 tests per processing step were carried out. After contact opening, the pin was stored and wear debris was collected by gently pressing a carbon adhesive tape on the block surface, out of the friction track. Pins,

blocks and tapes were then gold metalized to analyze the friction tracks and the debris morphology with a JEOL JSM-840 scanning electron microscope (SEM) operated at 20 kV.

2.2.3 Test campaign 3 (TC3): Welding tests and welded joint strength

The friction tests of TC3 were performed until the achievement of pin/block welding after different duration of friction. A total of 8 tests were performed with $MC = 11\%$, $P_C = 3.8$ MPa, and N ranging between 67 and 148 (that is, WT ranging from 1.3 to 2.9 s). The last friction coefficient recorded at the end of the test was named μ_{end}. Just after friction completion, a constant normal load of 200 N corresponding to $HP = 4$ MPa was maintained on the contact during $HT = 2$ min. After storage during 2 weeks under ambient air conditions ($T = 21 \pm 2°C$ and $RH = 42 \pm 8\%$), the 8 pin-on-block welded assemblies were then submitted to uniaxial tensile tests with a Lloyd LR30K apparatus in order to characterize their mechanical strength (σ). Among them, the internal structure of the welded assembly for which $N = 148$ was analyzed by X-ray tomography prior to mechanical testing using a GE Phoenix v|tome|xs equipment operated at 50 kV and 350 µA. Thanks to the small size of the samples, the characterizations were achieved without having to cut them off. As such, samples were prevented from additional cracks stemming from samples preparation that are traditionally encountered.[41] It resulted in a $10.3 \times 10.4 \times 1.5$ mm^3 stack of images composed of 5^3 µm^3 voxels which was then analysed using the Fiji software. As a reference, 5 pin/block pairs were assembled by applying 20 mg of conventional vinylic glue and then a constant 100 N normal load was maintained during 2 hours. After one week storage at ambient air, tensile tests were then carried out for comparison with the welded assemblies.

3 Results

3.1 Overall tribological behaviour

All friction tests performed in the framework of TC1 resulted in the typical evolution of the friction coefficient versus the number of friction cycles completed which is depicted with a black curve in Figure 2. This figure also shows the evolution of the mean normal load during a single friction cycle ($\overline{F_N}$) through a dotted line, and of the mean friction force during a single friction cycle ($\overline{F_T}$) through a grey line. The overall tribological behaviour can be subdivided into 4 successive steps which are delimited by the data points A, B and C appearing in Figure 2.
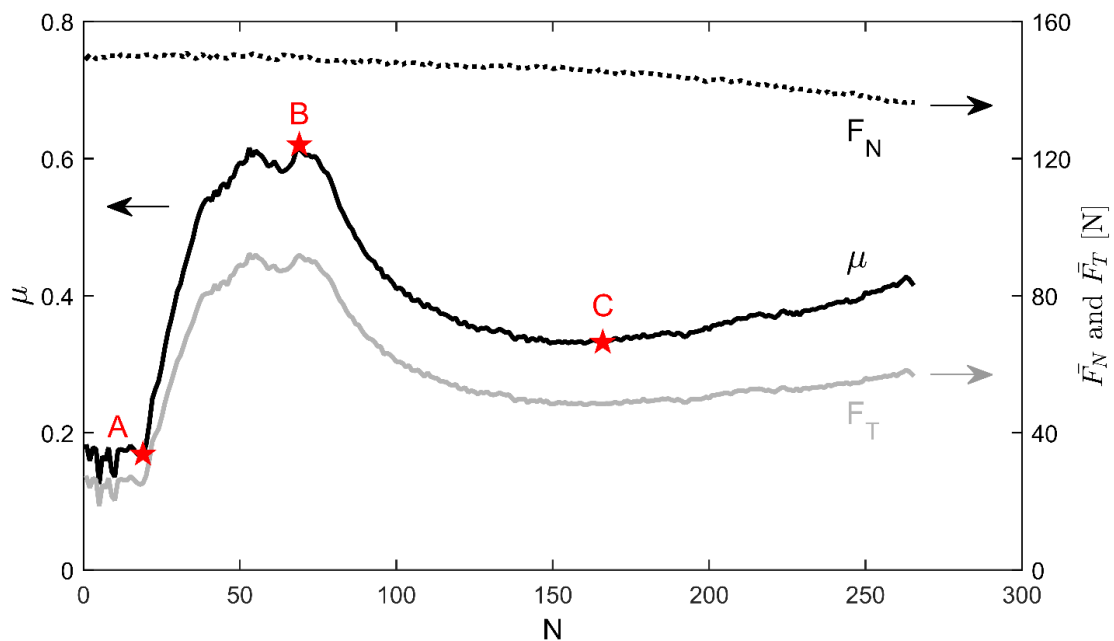
Figure 2:

At the very beginning of the test, μ remains low (close to 0.15) up to point A. The friction coefficient then drastically increases during a second step until reaching its maximum value in point B. This step is also accompanied by a clearly visible smoke production originating from the contact. Smoke production is a well-known phenomenon in FWW. In-depth characterization of emission gases achieved in previous studies revealed the existence of numerous volatile compounds but the major composition of smoke was found to be water vapour[34,40]. The third step (between B and C points) is characterized by a regular continuous decrease of μ according to a negative power law versus *N*, until reaching the local minimum value of μ in point C. It is worth mentioning that $\overline{F_N}$ starts to decrease from point B (Figure 2). Since normal load was applied through a tension spring, its decrease is then a direct indicator of wear. The slight decrease of $\overline{F_N}$ throughout the third step therefore reveals a mild wear process which is furthermore supported by the observation of wooden particles ejected from the contact. During the fourth step which starts from point C, the normal load decreases even more while μ increases. Notwithstanding, the friction coefficient increase during this step is not solely due to $\overline{F_N}$ decrease since an increase of $\overline{F_T}$ ranging from 4×10^{-2} to 1.2×10^{-1} N per friction cycle also occurs, depending on the initial contact pressure P_C. Figure 3 shows that the general trends of μ, $\overline{F_N}$, and $\overline{F_T}$ remains similar regardless of the contact conditions used.
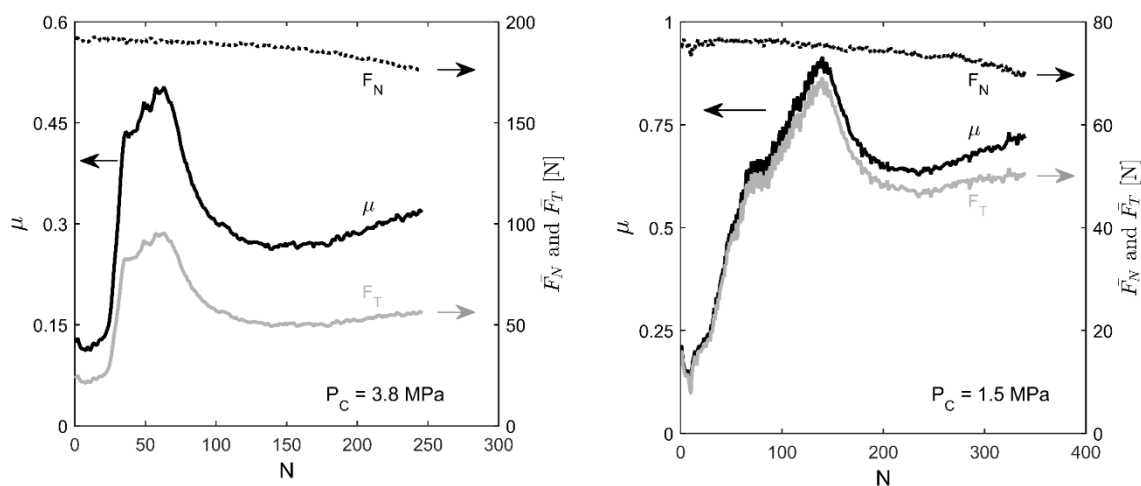
Figure 3:

Figure 3: Friction coefficient μ (black line), normal load F_N (dotted line), and friction force F_T (grey line) versus friction cycles number N with P_C = 3.8 MPa (left) and P_C = 1.5 MPa (right).

From point C, the simultaneous increase of $\overline{F_T}$ and decrease of $\overline{F_N}$ (cf Figures 2 and 3) is a direct evidence of the severe wear process occurring during the fourth step. This is also supported by the observed extensive extrusion of degraded wooden material pushed out of the contact. All the tests carried out within the TC1 framework were conducted beyond point C and resulted in an almost inexistent adherence between the pin and the block. Consequently, the fourth step must be considered as a separate process taking place in the continuity of FWW and defined as severe wear inducing the destruction of

the MZ previously formed. For this reason, the fourth step is not considered further in the followings sections.

3.2 Contact pressure (P_C) effect

The effect of the initial apparent contact pressure P_C on μ evolution is displayed in Figure 4. Friction curves have been plotted up to the point C defined in Figure 2 for the sake of clarity and to focus on the 3 first steps corresponding to FWW. For each contact conditions, the 5 tests performed shows relatively good reproducibility. It is assumed that differences are due to beech wood microstructure variations between samples despite the efforts made when selecting them.

Figure 4:
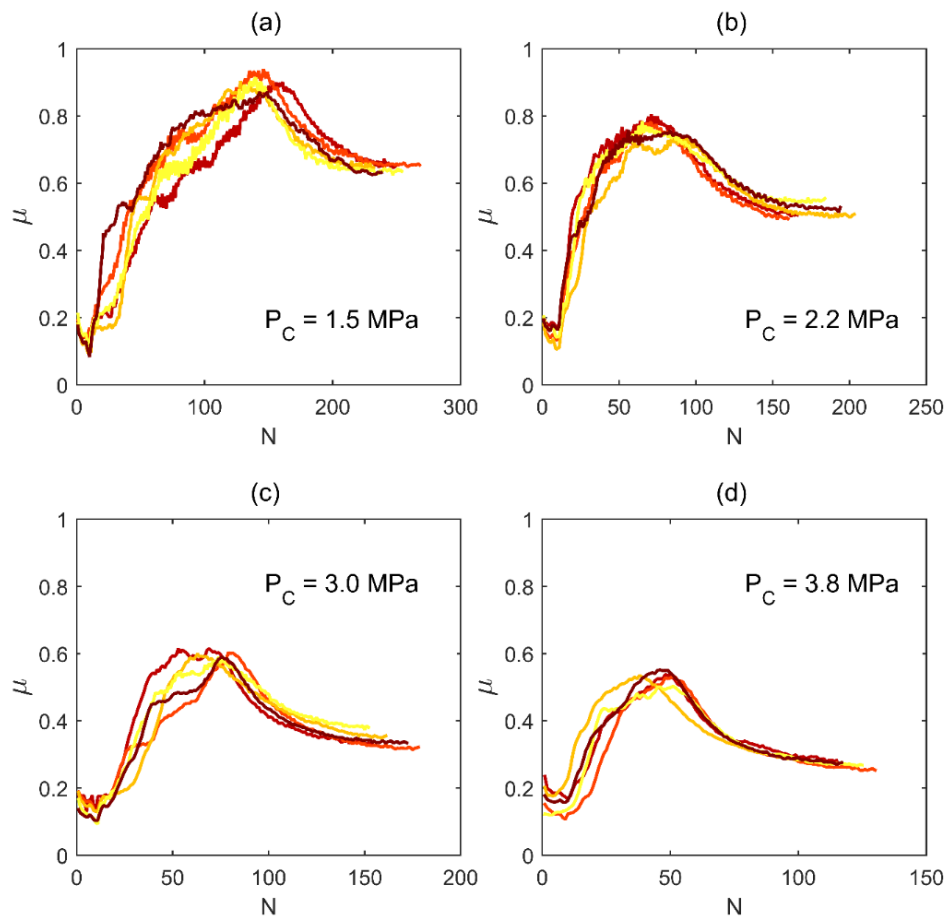
Figure 4: Friction coefficient μ (ordinate axes) versus friction cycles completed N (abscissa axes) until N_C for MC = 11% and P_C = 1.5 (a), 2.2 (b), 3.0 (c), and 3.8 MPa (d). Each graph shows 5 distinctive friction curves obtained with the same testing conditions. Note that μ results are not displayed according to the same range of N depending on the applied P_C value. (The reader is referred to the web version of this paper for colors visualization).

Figure 4 shows a similar trend of μ versus N for the 4 initial apparent contact pressures studied. Moreover, similar phenomena were observed during each test such as smoke production during the sharp increase of μ, and particles ejection during its further decrease. However, decreasing P_C leads to an overall increase of μ and an overall decay of the friction curve towards higher sliding distance. The

7

mean values of friction coefficients μ_A, μ_B, μ_C, and friction cycle numbers N_A, N_B, N_C related to the respective position of the points A, B, and C are so reported in Table 1.

Table 1:

P_C [MPa]	MC [%]	Number of friction cycles completed			Friction coefficient		
		N_A	N_B	N_C	μ_A	μ_B	μ_C
1.5	11	9 ± 9%	145 ± 12%	248 ± 6%	0.10 ± 16%	0.91 ± 3%	0.64 ± 2%
2.2	11	10 ± 5%	76 ± 13%	181 ± 10%	0.14 ± 16%	0.77 ± 4%	0.52 ± 5%
3.0	11	11 ± 4%	71 ± 8%	163 ± 10%	0.12 ± 16%	0.60 ± 2%	0.35 ± 5%
3.8	11	9 ± 8%	47 ± 9%	120 ± 10%	0.15 ± 16%	0.53 ± 3%	0.27 ± 4%
3.0	0	0	19 ± 10%	110 ± 10%	0.50 ± 7%	0.63 ± 1%	0.29 ± 6%
3.0	25	84 ± 17%	142 ± 11%	233 ± 13%	0.15 ± 11%	0.61 ± 6%	0.36 ± 6%

Table 1: Mean values (black written) and standard deviations (grey written) of the number of friction cycles completed N and the friction coefficient μ depending on P_C and MC, when positioning in the A, B, and C points defined in Figure 2.

For $MC = 11\%$, results highlight that point A position does not depend on P_C in terms of friction coefficient and of friction cycles number, while μ and N corresponding to points B and C tend to decrease as the contact pressure is increased. Notwithstanding, the decrease of μ is not only due to the normal load increase. To further investigate the frictional behavior of the contact at different steps of the FWW process, $\overline{F_T}$ versus $\overline{F_N}$ values at the 3 points A, B and C are plotted in Figure 5 for the 20 tests performed in TC1 with $MC = 11\%$.
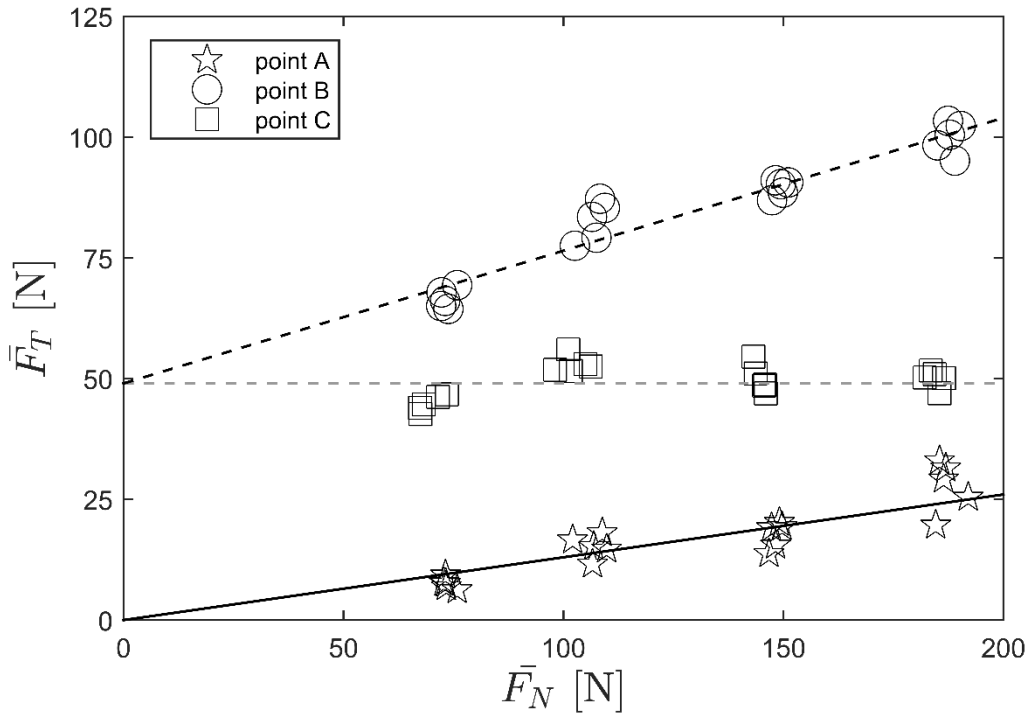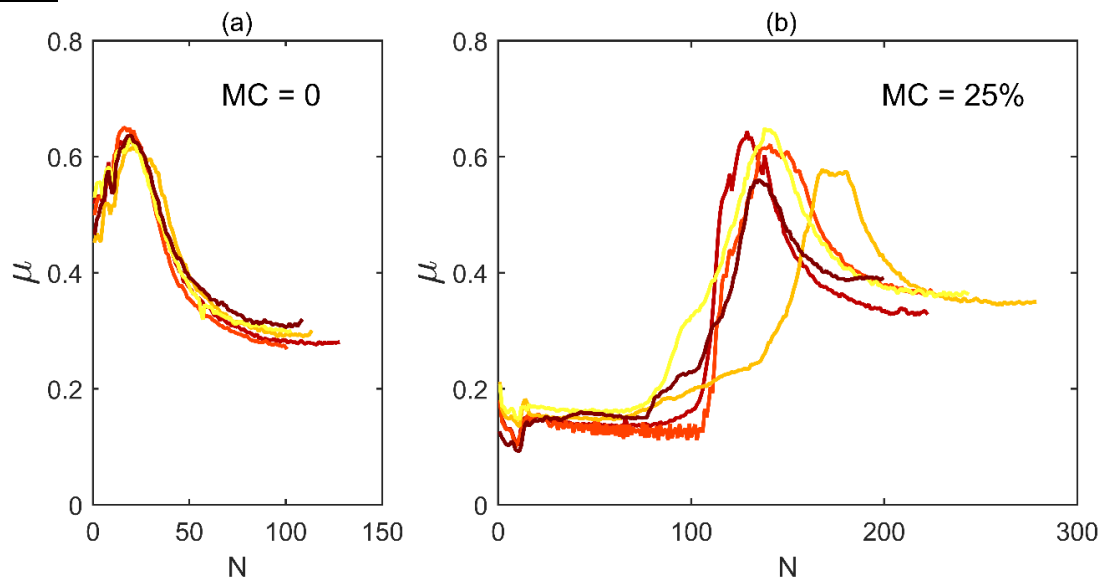
Figure 5:

Figure 5: Mean friction force $\overline{F_T}$ versus mean normal load $\overline{F_N}$ calculated at points A (stars), B (circles), and C (squares). Data refer to the 20 friction tests performed in TC1 with MC = 11%. Lines are linear regressions of the data corresponding to points A (black line), B (black dotted line), and C (grey dotted line).

Under the trustworthy assumption that friction mechanisms taking place respectively at points A, B and then C remains the same independently of P_C, Figure 5 helps to define the friction laws involved at different steps of FWW. Considering point A, the relationship between $\overline{F_T}$ and $\overline{F_N}$ is linear and intersects the origin of the graph. A very classical behaviour in accordance with the Amontons' laws is also observed at the very beginning of the test. The slope of the linear regression reaches 0.13 which is consistent with μ_A values listed in Table 1. When μ reaches its maximum at point B, $\overline{F_T}$ remains linearly correlated with $\overline{F_N}$ but the relationship does not pass through the origin of the graph, explaining the decrease of μ_B versus P_C. This relationship corresponds to the modified Coulomb law which suggests the addition of an adhesive component to the friction force. It is also suggested that a strong modification of the wooden contact rheology has already occurred at this stage of the process due to temperature increase, leading to an adhesive contact. When reaching point C, $\overline{F_T}$ remains constant, close to 50 N, whatever the initial contact pressure P_C applied. This surprising load-independence of the friction force shows that the tribological behaviour of the contact has been once again modified at this stage of the process. A further in-depth modification of the surfaces might be responsible of this. Interestingly, such an uncommon load-independency of the friction force was rarely observed in the literature, especially at the macroscopic scale, except for gels[42] or cellulose in aqueous solutions.[43]

3.3 Effect of wood samples moisture content (MC)

Figure 6 displays the evolution of μ versus N obtained when varying MC. All tests were achieved with $P_C = 3$ MPa and can be compared with results presented in Figure 4c where $MC = 11\%$. When $MC = 0$, the results highlight the absence of the first step corresponding to low friction. $N_A = 0$ must also be considered in this case. With anhydrous wooden parts, μ is close to 0.5 at the very beginning of the test and then immediately increases towards μ_B (Figure 6a). Moreover, it is worth mentioning that water vapour production was not observed in this case. In contrast, tests performed with $MC = 25\%$ are characterized by a significant increase of the duration of the low friction stage. As such, N_A ranges approximately from 80 to 100 (Figure 6b). Nonetheless, one can note that μ_A is not affected by MC. Similarly to the tests performed with $MC = 11\%$, water vapour production was observed during the sharp increase of μ between A and B points. These results highlight the lubricating action of water molecules trapped into the contact at the beginning of the test. When present, moisture ensures low friction forces and thus lowers the frictional heat generated in the contact, until water evaporation. With increasing MC, a longer sliding distance is therefore necessary to remove water molecules stored in the contact vicinity.

Figure 6:

9

From Figures 4c and 6, it is worth mentioning that increasing *MC* leads to lower tests reproducibility, especially between points A and B. Indeed, the standard deviations of the number of friction cycles achieved during the second step of the process (namely, N_B - N_A) reach 42% when *MC* = 25% while it drops to 10 and 13% when *MC* = 0 and 11%, respectively. To explain this variation, it is suggested that the higher the *MC*, the more heterogeneous the water evaporation rate is. Nonetheless, friction coefficients μ_B and μ_C remains nearly the same when *MC* varies from 0 to 25% (cf Table 1), meaning that the action of water molecules at the beginning of the test does not affect further the tribological behavior of the contact during the following steps of FWW.

3.4 Surface modifications

Tests performed in the framework of TC2 (P_C = 3 MPa and *MC* = 11%) highlight major surfaces modifications up to N_C. Figure 7 shows typical SEM observations of both friction tracks and wear debris when tests were successively interrupted close to N_B (*N* ranged from 55 to 67), between N_B and N_C (*N* ranged from 106 to 114), and close to N_C (*N* ranged from 164 to 175). Although pins were constantly rubbed whereas blocks experienced intermittent friction, their respective kinematic length are close resulting in similar surfaces modifications of the two wooden pairs.
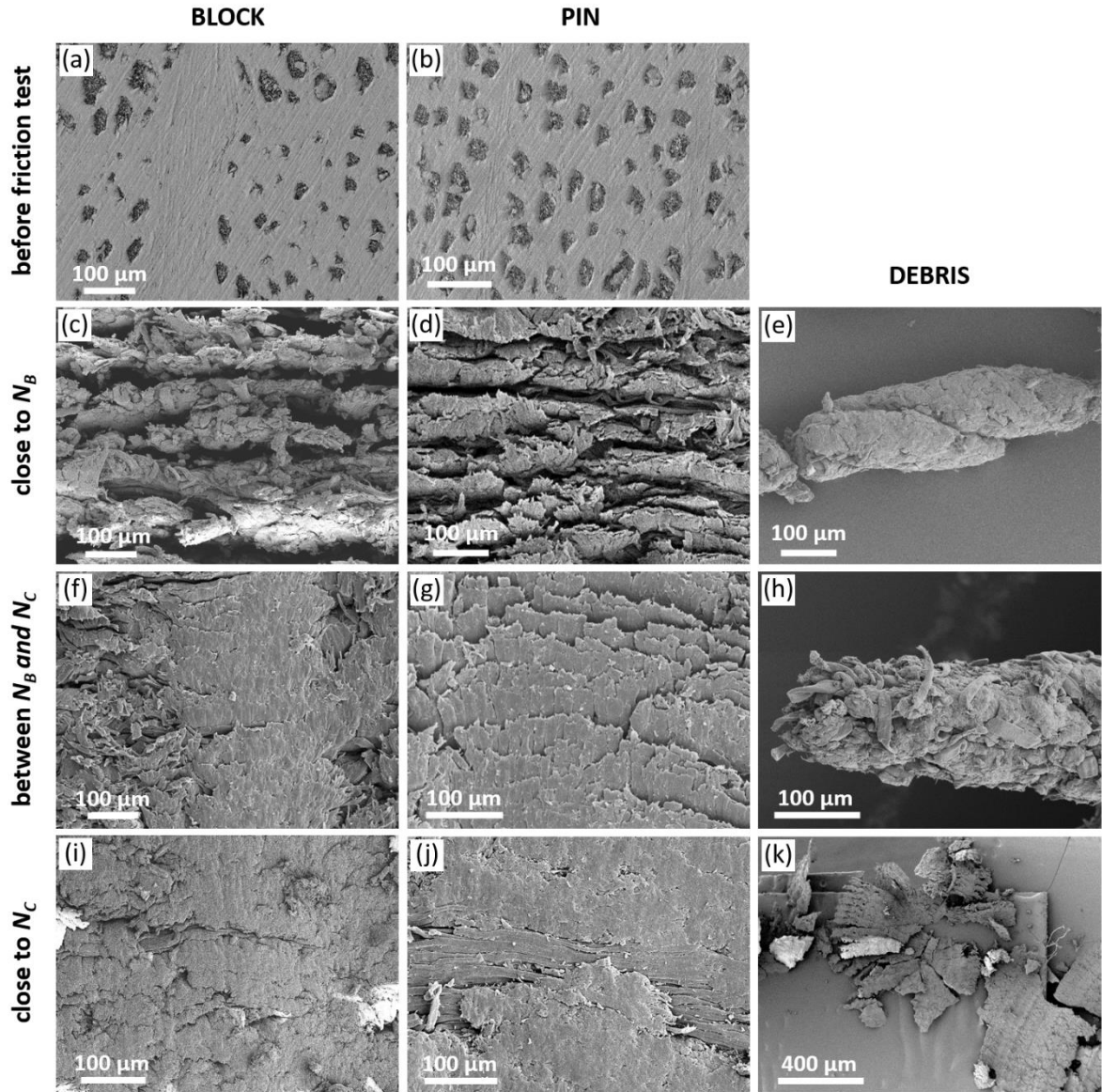
Figure 7:

Figure 7: SEM observations of the un-rubbed surfaces (a and b), of the block (c, f and i) and the pin (d, g and j) friction tracks, and of wear debris collected (e, h and k). Worn surfaces and debris stem from friction tests performed with $P_C = 3.0$ MPa and MC = 11%. SEM observations are related to tests stopped at different friction steps as defined in Figure 2: close to N_B (c to e), between N_B and N_C (f to h), and close to N_C (i to k). Considering block and pin tracks, the friction motion direction is vertical in all cases.

When μ has reached its maximum value (point B), Figures 7c and 7d show that both pin and block surfaces are highly damaged. The preexisting highly ordered diffuse-porous structure of beech wood (cf Figures 1d, 7a and 7b) is no longer observed due to the collapsing of the wood cell walls in the vicinity of the surface. One can observe that damaged fibers of beech wood are piled up in a direction mainly perpendicular to the pin motion. At this stage of FWW, large wear debris have been even produced. They exhibit a roll-shaped geometry which is several hundred micrometers long and several tens of micrometers in diameter. Figure 7e shows their building up through torsional shearing of a complex material composed of few damaged fibers stacked with molten matter. When the contact reaches approximately the middle of the process third step (Figures 7f and 7g), smoothening of both pin and block occurs through the spreading of the abovementioned damaged material onto the surfaces. SEM

11

observations display an overall plastic flow of the wooden material and show the on-set of melting in some surface zones disseminated over the friction track, such as the one observed in the center of Figure 7f. Wear debris collected at this stage of the process (Figure 7h) exhibit similar features than those collected close to N_B (Figure 7e) even though a higher fraction of damaged fibers seems to be embedded in the molten matrix. Notwithstanding, it is worth mentioning that debris collected at this stage could have been produced before, eventually close to N_B. At the end of the FWW third step (close to N_C), a covering of the whole pin and block surfaces by a molten material occurs, as evidenced in Figure 7i and 7j. Figure 7j particularly demonstrates that the molten material layer spreads over undamaged wood fibers. Interestingly, wear debris evacuated from the contact at this stage of the process are radically different from the previous ones. As shown in Figure 7k, very large platelets are extracted from the contact. They reach up to 500 µm in length and width and appear to result from the shearing of the melting zone.

3.5 Welded joint structure and strength

In contrast to experiments presented above, tests performed in the framework of TC3 were carried out in order to successfully achieve welding of the two wooden parts. Since previous results suggested the onset of the MZ formation from point B and the initiation of a severe wear process from point C, friction tests were therefore stopped at various N values ranging from N_B and N_C. The friction coefficient reached at the end of each experiment were named μ_{end} and each contact pairs were then maintained during $HT = 2$ min and under $HP = 4$ MPa to achieve welded joint solidification. Figure 8 displays the X-ray computed tomography analysis performed in the particular case of the welded assembly obtained with $N = 148$ and $\mu_{end} = 0.27$. From the reconstructed 3D block corresponding to the whole assembly, cross-sections of the pin/block interface perpendicular to the friction motion direction are presented in Figures 8b to 8e. The selected cross-sections only display the structure of the mid-contact area since a similar one was observed on the other side of the contact.
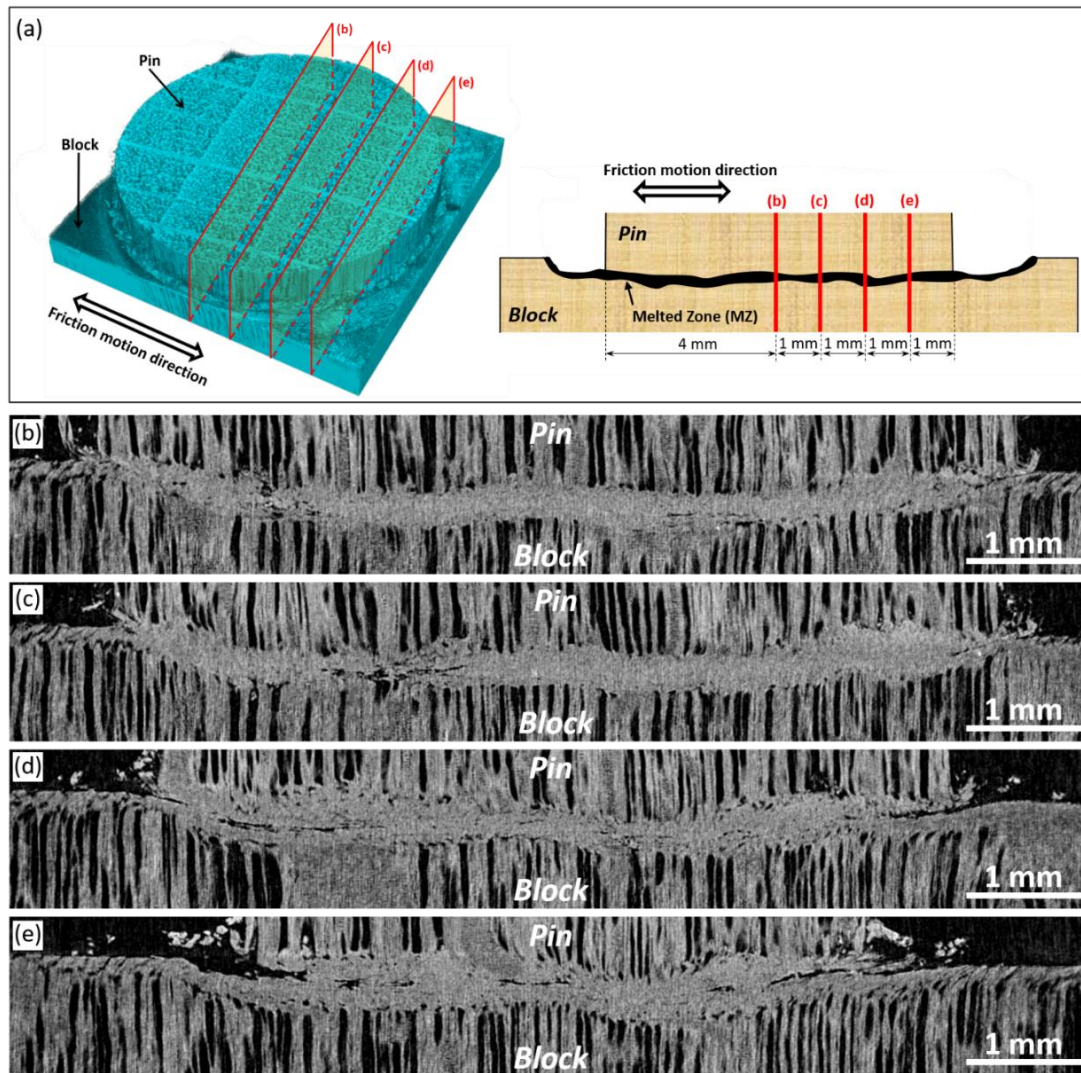
Figure 8:

Figure 8: (a) 3D reconstructed pin/block contact obtained by X-ray computed tomography after a friction test performed in TC3 (PC = 3.8 MPa, MC = 11%, N = 155, μ_{end} = 0.27, HT = 2 min, HP = 4 MPa), and scheme indicating the location of the 4 reconstructed cross-sections of the welded assembly (b to e).

Observation of every reconstructed cross-sections confirms the formation of a thick MZ consecutively to the third body spreading and curing. Measurements of the MZ thickness in various locations led to a mean value of 260 ± 87 µm. Although slightly larger, this mean thickness is in agreement with other studies focused on beech wood.[11,31,41] The welded interface clearly results in a greatly densified zone compared to the original bulk wood structure, as previously mentioned in the literature.[11,21,31] The welded joint in the centre of the contact (Figure 8b) appears relatively homogeneous despite some porosities and local thinning of the MZ are observed. Nonetheless, the further away from the centre, the greater the occurrences of porosities, welded joint disruptions, and cracks are (Figures 8c to 8e). Although the present study does not focus on the joint strength maximization, such observations support the concept that an optimization of the contact conditions should minimize structural defects of the MZ to reach higher strength, as requested by previous studies.[16,20,22,23] Conversely, Figures 8b to 8e evidence the local filling of bulk wood voids by the third body which should result in a structural reinforcement of the assembly.

Tensile tests performed on the 8 assemblies originating from TC3 resulted in mechanical strengths (σ) up to 7 MPa. Similar values were reported in the literature for beech[21] and birch[20] welded using almost

13

the same contact conditions. Figure 9 shows the effect of test duration on the tensile strength of pin/block welded assemblies. The results are compared with the mean strength of glued assemblies (grey lines in Figure 9), and are reported versus N or versus μ_{end} in Figures 9a and 9b, respectively. It is worth mentioning that the highest mechanical strengths reached by the welded assemblies are close to the ones obtained with glued assemblies.
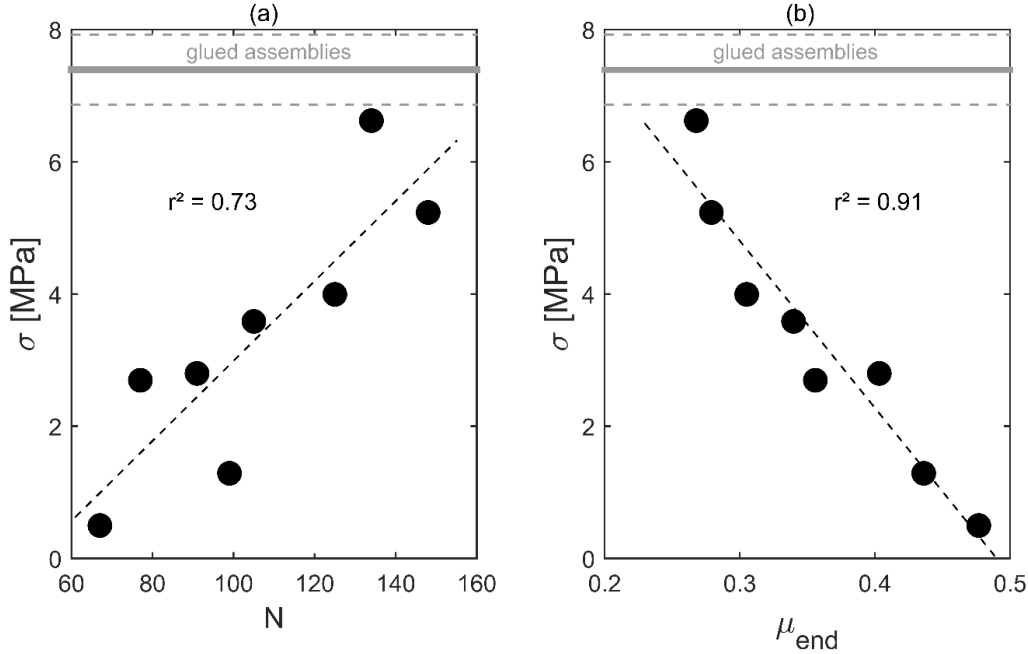
Figure 9:

Figure 9: Tensile strength σ of joints obtained after various welding time WT performed with $P_C = 3.8$ MPa, MC = 11%, HP = 4 MPa, and HT = 2 min. Results are plotted versus the number of friction cycles completed N (left), and the last friction coefficient recorded μ_{end} (right). The grey horizontal thick line refers to the mean tensile strength measured on glued wooden parts assemblies and the grey horizontal dotted lines refer to its ± ½ standard deviation. Linear regressions (black dotted lines) and associated correlation factors r² are indicated for each graph.

The general trend highlighted in Figure 9a shows that the closer to point C the friction motion has been stopped, the higher the mechanical strength is. This observation is consistent with the above-mentioned gradual spreading of the melted third body onto the surfaces. It is also suggested that higher third body spreading leads to more homogeneous distribution of the *MZ* along the contact, and consequently to higher assembly strength after solidification. Nonetheless, scattered tensile strength values were obtained as a function of N ($r^2 = 0.73$). By contrast, Figure 9b exhibits a better linear correlation factor between σ and μ_{end} ($r^2 = 0.91$). The observed negative slope reflects the achievement of smaller and smaller friction coefficients as the third body spreads into the contact during the third step of FWW, as depicted in Figures 2 to 4.

It is assumed that better correlation between σ and μ_{end} than with N relies on the inherent structural heterogeneity of wood. As such, two different samples are likely to reach different interface states after performing the same sliding distance. By contrast, the same friction coefficient should refer to the same MZ rheology resulting in similar strength of the assembly further to MZ solidification. This assumption is supported by variation of the friction curves depicted in Figure 4 and 6 for each contact conditions, which is quantified by the higher standard deviations of N_B and N_C compared to those of μ_B and μ_C as reported in Table 1.

4 Discussion

To the best of our knowledge, the present study provides the first approach to FWW from a tribological perspective. In particular, the first values and the evolution of the friction coefficient acquired during the linear welding of wooden pairs are presented. The results demonstrate a very specific inverted U-shaped friction curve looking like the one proposed by Stamm *et al* in the particular case of orbital welding.[8] However, higher friction coefficients were found and an unrevealed dependence of the normal loading was encountered. Such differences can primarily be explained by the radically different contact modalities employed. Considering linear welding, contact conditions used in the present study are similar to those used by Boonstra *et al*[21], but they refer to lower sliding speed (SV) and higher contact pressure (WP) compared with the most common welding conditions used in the literature. The combination of friction measurements under different contact conditions (P_C and MC), of surface modifications at different steps of the process, and of the resulting welded joint characterization allows for an extensive description of the tribological mechanisms involved during FWW. Interestingly, these mechanisms are very exhaustive. They are summarized phenomenologically in Figure 10 and discussed in the followings.

At the very beginning of the process, the friction is low. When varying P_C from 1.5 to 3.8 MPa, the plot of $\overline{F_T}$ versus $\overline{F_N}$ shows a classical relationship reflecting the Amonton's law (Figure 5). The friction coefficient does not depend on the apparent contact pressure and reaches 0.13 approximately. This low value has been attributed to the lubricating action of water molecules trapped into the contact and originating from the moisture initially contained in the beech wood samples (Figure 10a). Indeed, tests performed with anhydrous samples led to four times higher friction coefficient at this stage (Figure 6a). From the literature, the role of moisture on the frictional behavior of wood surfaces remains however not well understood and highly depends on the material counterpart considered.[44–47] Referring to the well-known Stribeck curve, the friction coefficient load-independence encountered in the present study suggests that boundary lubrication occurs. Such a lubrication regime is consistent with the small amount of water involved and its low viscosity. Nonetheless, increasing MC does not change μ. This behaviour was previously observed with wood rubbing on a PTFE counterpart[45], until $MC = 30\%$. Notwithstanding, the duration of the low-friction regime highly increases with MC (Figure 6b). This suggests the material acts like a "water-tank" which is gradually depleted by frictional heating.

Thereafter, the contact is no longer lubricated since water vaporizes due to the heat generated by friction. Evidence of water vaporization was observed in the present study through clearly visible smoke production that was also reported in the literature.[2,8,34,40] This results in a very sharp increase in the friction coefficient since the absence of aqueous lubricant leads to severe surface damage (Figure 10b), as shown in Figures 7a and 7b. The friction coefficient then reaches its maximal level μ_B which decreases with P_C, as reported in Table 1 and Figure 4. Such behaviour refers to a strong modification of the contact rheology at this step of the process. This statement is consistent with the work of Ganne-Chedeville *et al* arguing that wood becomes rubber-like at the first stages of FWW through the combined action of the temperature and of the chemically-driven decrease of the glass transition temperature of lignin.[31] While differing in terms of sliding speed and contact pressures compared to those employed in the present study, welding tests performed by the authors of this paper were combined with infrared thermography measurements that allowed to suggest the occurrence of numerous physicochemical phenomena. Based on their observations, the second step of FWW (from point A to point B) should comprise: molecular swelling of the polysaccharides, increase of the lignin molecules flexibility, and hydrolysis of the hemicelluloses and the amorphous cellulose. At the end of the second step, the $\overline{F_T}$ versus $\overline{F_N}$ relationship (Figure 5) suggests the existence of an adhesive term in the friction force as suggested by Atack and Tabor[45] who studied balsam wood. As a complex mixture of macromolecular organic constituents, the frictional behaviour of wood can also be compared to that of polymers. Briscoe *et al*[48–50] showed the friction law of such materials can be expressed as follows:

$$F_T = A\,\tau_0 + \alpha\,F_N \qquad \text{(Eq.2)}$$

where A is the real contact area, and α and τ_0 are constants. Data from Figure 5 give $\alpha = 0.28$ and assuming A close to the apparent contact area gives $\tau_0 \approx 1$ MPa, that are consistent values very similar to those obtained for thermoplastics.[48] Such consideration supports the adhesive nature of the interface at this stage of the process.
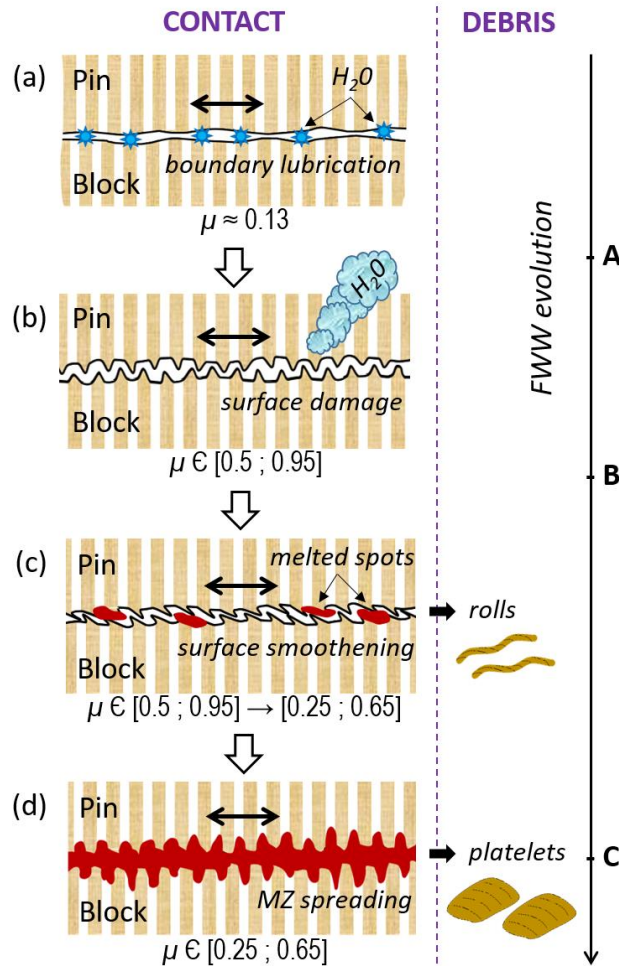
Figure 10:

Figure 10: Surface modifications involved throughout FWW. When indicating as an interval, µ values refer to their variations depending on P_C. The arbitrary time scale (right side) indicates the points A, B and C defined in Figure 2.

During the third step of FWW (between points B and C) the friction coefficient decreases according to a negative power law versus N. SEM observations (Figure 7) indicate that such behaviour first relies on plastic flow that induces surface smoothening, and the onset of melted spots (Figure 10c) that gradually spread on the surfaces to further achieve the MZ growing up. Based on the literature, these physical processes can be connected with cellulose dehydration and decarboxylation leading to its depolymerisation[31], and the partial melting of lignin and hemicelluloses.[2,39] Meanwhile, large roll-shaped debris are ejected from the contact. In contrast with isolated wood cells observed by Gfeller *et al*[2], wear debris collected in our experiments are composed of fragmented wood fibres embedded in a molten matrix. Observation of such debris composition close to point B supports the emergence of molten material spots from the very beginning of the FWW third step. All of these observations support the reaching of a mixed lubrication regime. From Figure 8, X-ray tomographic analysis performed on a contact pair whose friction was maintained close to point C highlights that a thick MZ was ultimately built up at the end of this stage (Figure 10d). High thickness of the resulted MZ similar to the one

observed by Boonstra *et al* under similar contact conditions[21] raises the question of whether the contact reaches, or not, the hydrodynamic (or elasto-hydrodynamic) lubricating regime at the end of the third step. The following interpretation is based on the assumption that the interface at point C is in the same state and also has the same viscosity whatever P_C. On the one hand, assuming low variations of the contact area in the F_N range considered, hydrodynamic lubrication should be characterized by friction forces proportional to $F_N{}^{1/4}$, including in the case of materials lubricated by their own melting.[51,52] However, Figure 5 shows $\overline{F_T}$ does not depend on $\overline{F_N}$ and reaches a constant value. On the other hand, increasing P_C results in decreasing the friction coefficient which remains relatively high, from 0.25 to 0.65 (Table 1). Such observations, also related to the Stribeck curve, are consistent with the perpetuation of the mixed lubrication regime originated since point B. A significant quantity of molten material should nonetheless be present in the contact. As already mentioned in the literature[3], one part of this fluid-like material cannot be kept trapped any longer into the contact and is pushed out of the contact. It is then quickly cured to generate large platelets as depicted in Figure 7k. Conversely, another part of the molten material fills the beech wood structural voids owed to the end grain-to-end grain orientation of the samples (Figure 8). This also tends to enhance the mechanical strength of the resulting assembly. Continuing friction tests beyond point C initiates severe wear of the wooden samples and causes a very weak connection and even no adherence between the pin and the block in most cases. Although not in the scope of the present paper, the wear process is manifested by extensive extrusion of the molten material previously formed. As such, it can be seen as an exacerbated continuation of the FWW third step ending. Meanwhile, furfural-derived products resulted from the heat degradation of hemicelluloses appear through condensation reactions involving glucose and xylose[31,39], and the pyrolysis of holocellulose is suggested to occur.[31] Moreover, as mentioned by Vaziri *et al*[19], longer welding time also causes the occurrence of charring in the welded zone which ultimately decreases even more the assembly strength.

In addition to the identification of the tribological mechanisms involved in FWW, the present study highlights the relevance of the friction coefficient as an effective tool for controlling the process. Firstly, one must consider the large variation of the friction curve during a single test. Indeed, μ is more than quadrupled throughout a same test and can even vary by almost a decade under low contact pressure (Figure 4 and Table 1). As a quantitative indicator of the interface rheology, the friction coefficient is also a precise monitoring parameter in order to evaluate the progression of welding achievement. Despite efforts made to limit the structural heterogeneity of the samples (see section 2.1), the five friction curves obtained for each contact conditions of TC1 showed some variations of the necessary sliding distance to reach a specific interface state (Figures 5 and 6). This was especially observed with increasing moisture content (Figure 6b). In contrast, a better reproducibility was observed when considering the friction coefficient levels as proved by the low standard deviations exhibited by μ_B and μ_C (Table 1) in each contact conditions. Moreover, since the overall process is achieved in a few seconds, μ also offers a precious tool to quickly distinguish the successive steps of the interface modifications. Secondly, our results suggest that the mechanical strength of the resulting assembly could be efficiently predicted with μ. The linear relationship depicted in Figure 9b between μ_{end} and σ is of major concern from a practical point of view for the achievement of the process. In all previous studies, FWW is usually controlled with definite *WT* and motion frequency that means a fixed sliding distance. However, the comparison of Figures 9a and 9b shows that σ could be more precisely controlled by monitoring the friction coefficient than *N*.

5   Conclusion

This study aims at providing the first study on friction wood welding through a tribological approach. The work carried out includes friction tests performed on beech wood and mechanical and morphological characterizations of the interface thanks to different techniques. The main findings from this study are listed below.

(1) The evolution of the friction coefficient during linear wood welding process was provided for the first time. After a low-friction stage, the friction coefficient follows an inverted U-shaped curve versus the sliding distance through a second stage.

(2) Despite the very short duration of the process, very large variations of the friction coefficient ranging from 0.1 to 1 were observed.

(3) Friction curves strongly depend on the initial apparent contact pressure and the moisture content of wood. Increasing the pressure leads to lower friction coefficients during the second stage, and the wood moisture content acts on the duration of the first step until its vanishing with anhydrous wood.

(4) This study highlights the richness of tribological mechanisms involved in FWW. It was demonstrated that the wooden interface successively experiences (i) boundary lubrication regime governed by water molecules trapped in the contact, (ii) adhesive dry friction, (iii) mixed lubrication regime piloted by the gradual spreading of a molten material, and then (iv) severe wearing of the contact due to the removal of the previously formed molten material.

(5) From an industrial perspective, our work points out the relevance to follow the friction coefficient throughout FWW as a relevant and predictive measurement of both the process progression and the optimization of the welded assembly mechanical strength.

The present study focuses on the welding of beech wood under a single sliding speed. Further works have to be carried out to investigate whether the abovementioned tribological mechanisms vary with different sliding speeds and wood species.

6   Acknowledgement

7   References

1. Sutthoff, B., Franz, U., Hentschel, H., & Schaaf, A. Patentschrift DE 196 20 273 C2. (1996).
2. Gfeller, B. *et al.* Wood bonding by vibrational welding. *J. Adhes. Sci. Technol.* **17,** 1573–1589 (2003).
3. Gfeller, B. *et al.* Wood Bonding by Mechanically-Induced in situ Welding of Polymeric Structural Wood constituents. *J. Appl. Polym. Sci.* **92,** 243–251 (2004).
4. Tondi, G., Andrews, S., Pizzi, A. & Leban, J. M. Comparative potential of alternative wood welding systems, ultrasonic and microfriction stir welding. *J. Adhes. Sci. Technol.* **21,** 1633–1643 (2007).
5. Pizzi, A., Leban, J. M., Kanazawa, F., Properzi, M. & Pichelin, F. Wood dowel bonding by high-speed rotation welding. *J. Adhes. Sci. Technol.* **18,** 1263–1278 (2004).
6. Ganne-Chedeville, C. *et al.* Parameter interactions in two-block welding and the wood nail concept in wood dowel welding. *J. Adhes. Sci. Technol.* **19,** 1157–1174 (2005).
7. Stamm, B., Natterer, J. & Navi, P. Joining of wood layers by friction welding. *J. Adhes. Sci. Technol.* **19,** 1129–1139 (2005).
8. Stamm, B., Natterer, J. & Navi, P. Joining wood by friction welding. *Holz als Roh- und Werkst.* **63,** 313–320 (2005).
9. Omrani, P., Mansouri, H. R. & Pizzi, A. Influence of wood grain direction on linear welding. *J. Adhes. Sci. Technol.* **23,** 2047–2055 (2009).
10. Omrani, P., Mansouri, H. R. & Pizzi, A. Linear welding of grooved wood surfaces. *Eur. J. Wood Wood Prod.* **67,** 479–481 (2009).
11. Leban, J.-M. *et al.* X-ray microdensitometry analysis of vibration-welded wood. *Holzforschung* **58,** 45–52 (2004).

12. Gfeller, B. *et al.* Solid wood joints by in situ welding of structural wood constituents. *Holzforschung* **58,** 45–52 (2004).

13. Properzi, M. *et al.* Influence of grain direction in vibrational wood welding. *Holzforschung* **59,** 23–27 (2005).

14. Rautkari, L., Properzi, M., Pichelin, F. & Hughes, M. Surface modification of wood using friction. *Wood Sci. Technol.* **43,** 291–299 (2009).

15. Hahn, B., Stamm, B. & Weinand, Y. Influence of surface shapes on the mechanical behaviour of friction welded wood bonds. *Eur. J. Wood Wood Prod.* **73,** 29–34 (2015).

16. Amirou, S., Pizzi, A. & Luo, H. Variation of shear properties of welded spruce at different pressures and welding times. *Biotribology* **5,** 61–66 (2016).

17. Mansouri, H. R. *et al.* Causes for the Improved Water Resistance in Pine Wood Linear Welded Joints. *J. Adhes. Sci. Technol.* **25,** 1987–1995 (2011).

18. Vaziri, M., Berg, S., Sandberg, D. & Gheinani, I. T. Three-dimensional finite element modelling of heat transfer for linear friction welding of Scots pine. *Wood Mater. Sci. Eng.* **9,** 102–109 (2014).

19. Vaziri, M., Lindgren, O. & Pizzi, A. Influence of welding parameters and wood properties on the water absorption in Scots pine joints induced by linear welding. *J. Adhes. Sci. Technol.* **25,** 1839–1847 (2011).

20. Ruponen, J. *et al.* Influence of welding time on tensile-shear strength of linear friction welded birch (Betula pendula L.) wood. *BioResources* **10,** 3481–3491 (2015).

21. Boonstra, M. *et al.* Vibration welding of heat-treated wood. *J. Adhes. Sci. Technol.* **20,** 359–369 (2006).

22. Belleville, B., Amirou, S., Pizzi, A. & Ozarska, B. Optimization of Wood Welding Parameters for Australian Hardwood Species. *BioResources* **12,** 1007–1014 (2017).

23. Martins, S. A., Ganier, T., Pizzi, A. & Del Menezzi, C. H. S. Parameter scanning for linear welding of Brazilian Eucalyptus benthamii wood. *Eur. J. Wood Wood Prod.* **71,** 525–527 (2013).

24. Mansouri, H. R., Pizzi, A. & Leban, J. M. End-grain butt joints obtained by friction welding of high density eucalyptus wood. *Wood Sci. Technol.* **44,** 399–406 (2010).

25. Zhang, H., Pizzi, A., Lu, X. & Wang, Z. Study of the End-grain butt joints obtained by friction welding of moso bamboo. *BioResources* **12,** 6446–6457 (2017).

26. Zhang, H., Pizzi, A., Zhou, X., Lu, X. & Wang, Z. The study of linear vibrational welding of moso bamboo. *J. Adhes. Sci. Technol.* **32,** 1–10 (2017).

27. Zigon, J. *et al.* The influence of heat and chemical treatments of beech wood on the shear strength of welded and UF bonded specimens. *Eur. J. Wood Wood Prod.* **73,** 685–687 (2015).

28. Omrani, P., Mansouri, H. R., Duchanois, G. & Pizzi, A. Fracture mechanics of linearly welded wood joints: Effect of wood species and grain orientation. *J. Adhes. Sci. Technol.* **23,** 2057–2072 (2009).

29. Mansouri, H. R., Omrani, P. & Pizzi, A. Improving the water resistance of linear vibration-welded wood joints. *J. Adhes. Sci. Technol.* **23,** 63–70 (2009).

30. Amirou, S., Pizzi, A. & Delmotte, L. Citric acid as waterproofing additive in butt joints linear wood welding. *Eur. J. Wood Wood Prod.* **75,** 651–654 (2017).

31. Ganne-Chédeville, C., Properzi, M., Leban, J. M., Pizzi, A. & Pichelin, F. Wood welding: Chemical and physical changes according to the welding time. *J. Adhes. Sci. Technol.* **22,** 761–773 (2008).

32. Ganne-Chédeville, C. *et al.* Wood welded connections: Energy release rate measurement. *J. Adhes. Sci. Technol.* **22,** 169–179 (2008).

33. Vaziri, M., Lindgren, O. & Pizzi, A. Influence of weldling parameters on weldline density and its relation to crack formation in welded Scots pine joints. *J. Adhes. Sci. Technol.* **25,** 1819–1828 (2011).

34. Omrani, P., Masson, E., Pizzi, A. & Mansouri, H. R. Emission gases in linear vibration welding of wood. *J. Adhes. Sci. Technol.* **23,** 85–94 (2009).

35. Omrani, P., Pizzi, A., Mansouri, H. R., Leban, J. M. & Delmotte, L. Physico-chemical causes of the extent of water resistance of linearly welded wood joints. *J. Adhes. Sci. Technol.* **23,** 827–837 (2009).

36. Vaziri, M., Lindgren, O., Pizzi, A. & Mansouri, H. R. Moisture sensitivity of scots pine joints

produced by linear frictional welding. *J. Adhes. Sci. Technol.* **24,** 1515–1527 (2010).

37. Pizzi, A. *et al.* Enhancing water resistance of welded dowel wood joints by acetylated lignin. *J. Adhes. Sci. Technol.* **27,** 252–262 (2013).

38. Ganne-Chédeville, C., Duchanois, G., Pizzi, A., Leban, J.-M. & Pichelin, F. Predicting the Thermal Behaviour of Wood During Linear Welding Using the Finite Element Method. *J. Adhes. Sci. Technol.* **22,** 1209–1221 (2008).

39. Delmotte, L., Ganne-Chedeville, C., Leban, J. M., Pizzi, A. & Pichelin, F. CP-MAS 13C NMR and FT-IR investigation of the degradation reactions of polymer constituents in wood welding. *Polym. Degrad. Stab.* **93,** 406–412 (2008).

40. Omrani, P., Masson, E., Pizzi, A. & Mansouri, H. R. Emission of gases and degradation volatiles from polymeric wood constituents in friction welding of wood dowels. *Polym. Degrad. Stab.* **93,** 794–799 (2008).

41. Vaziri, M., Plessis, A. Du, Sandberg, D. & Berg, S. Nano X-ray tomography analysis of the cell-wall density of welded beech joints. *Wood Mater. Sci. Eng.* **10,** 368–372 (2015).

42. Gong, J., Higa, M., Iwasaki, Y., Katsuyama, Y. & Osada, Y. Friction of Gels. *J. Phys. Chem. B* **101,** 5487–5489 (2002).

43. Zauscher, S. & Klingenberg, D. J. Friction between cellulose surfaces measured with colloidal probe microscopy. *Colloids Surfaces A Physicochem. Eng. Asp.* **178,** 213–229 (2001).

44. Svensson, B. A., Nyström, S., Gradin, P. A. & Höglund, H. Frictional testing of wood-Initial studies with a new device. *Tribol. Int.* **42,** 190–196 (2009).

45. Atack, D. & Tabor, D. The friction of wood. *Proc. R. Soc. London. Ser. A. Math. Phys. Sci.* **246,** 539–555 (1958).

46. McKenzie, W. M. Friction coefficient as a guide to optimum rake angle in wood machining. *Wood Sci. Technol.* **25,** 397–401 (1991).

47. McMillin, C. W., Lemoine, T. J. & Manwillel, F. G. Friction coefficient of oven-dry spruce pine on steel, as related to temperature and wood properties. *Wood Fiber Sci.* 6–11 (1970).

48. Amuzu, J. K. A., Briscoe, B. J. & Tabor, D. Friction and shear strength of polymers. *ASLE Trans.* **20,** 354–358 (1977).

49. Briscoe, B. J. & Tabor, D. The Effect of Pressure on the Frictional Properties of Polymers. *Wear* **34,** 29–38 (1975).

50. Briscoe, B. J. & Tabor, D. Shear Properties of Thin Polymeric Films. *J. Adhes.* **9,** 145–155 (1978).

51. Beretta, G. P., Niro, A. & Silvestri, M. Solid Slider Bearings Lubricated by Their Own Melting or Sublimation. *Journla Tribol.* **109,** 296–300 (1987).

52. Stiffler, A. K. Friction and Wear With a Fully Melting Surface. *J. Tribol.* **106,** 416–419 (1984).